Chemie Ingenieur Technik

Chemie Ingenieur Technik

RESEARCH ARTICLE OPEN ACCESS

Energy Flexibilization and Demand Response for a Novel Decentralized Power-to-Methanol Process

Max Kollmer[1] | Markus Vogelbacher[1] | Mücahit Terzi[2] | Mohit Singh[2] | Francsico Vidal-Vazquez[3] | Jörg Matthes[1]

[1]Institute for Automation and Applied Informatics, Karlsruhe Institute of Technology, Eggenstein-Leopoldshafen, Germany | [2]Institute for Micro Process Engineering, Karlsruhe Institute of Technology, Eggenstein-Leopoldshafen, Germany | [3]ICODOS GmbH, Mannheim, Germany

Correspondence: Max Kollmer (max.kollmer@kit.edu)

Received: 2 September 2025 | **Revised:** 27 March 2026 | **Accepted:** 27 March 2026

Keywords: demand response | PtM | PtX | scheduling

ABSTRACT

Due to the rising share of renewables, demand response is becoming more important. Power-to-X technologies are suitable for storing excess energy, due to their high flexibility and fast ramping capabilities. This work presents an optimization framework for the flexibilization of a power-to-methanol process. Based on simulation data from stationary operating points, a mixed-integer nonlinear program including buffer storage, an electrolyser, a PV system, a battery and a PtM plant is constructed. The optimal operation for minimum operating costs and CO_2 emissions is determined considering dynamic electricity prices, varying renewable electricity supply and self-sufficient operation. The results demonstrate flexible operation reduces costs by over 30% and the CO_2 footprint by up to 24%. In self-sufficient mode, flexible operation allows continuous operation, while stationary operation leads to frequent shutdowns and a lower methanol yield.

1 | Introduction

Green methanol production is a promising process to use surplus renewable electricity to produce methanol through flexible operation. Interest in this climate-neutral technology has risen sharply due to the growing demand for methanol, both as a chemical feedstock and an alternative fuel [1, 2]. To utilize possible flexibilization potentials of the power-to-methanol (PtM) process, strategies like demand response and optimal scheduling are becoming increasingly important [3]. Numerous studies in energy-intensive industries have explored these topics. For instance, several works [4, 5] investigated a chlorine production process with two operation modes, whereby the greatest savings were achieved through oversizing and mode switching. Ref. [6] developed a demand response–oriented model for a chlor-alkali process and achieved a reduction in electricity costs and load curtailment during peak electricity prices. Ref. [7] applied demand response and cost optimization to two steel plants based on future electricity prices, storage sizes and other flexibility parameters, achieving cost savings of up to 35%. In cement production, [8] examined the demand response potential with reinforcement learning methods and verified the results with simulation data. Ref. [9] investigated the effect of different demand response programs on three cement plants based on a mathematical model and data from the plants. The production scheduling under uncertainty of an air separation unit is examined in [10], while [11] modeled the scheduling of an air separation unit as a mixed-integer linear problem (MILP) with a novel dynamic modeling strategy, achieving significant reductions in operating costs and peak power demand. Ref. [12] investigated the production scheduling of air separation units with data-driven methods to balance the power grid.

Abbreviations: LHHW, Langmuir–Hinshelwood–Hougen–Watson; MILP, mixed-integer linear problem; MINLP, mixed-integer nonlinear problem; NRTL, non-random two-liquid; PC-SAFT, perturbed chain-statistical associating fluid theory; PtM, power-to-methanol; PtX, power-to-X; RWGS, reverse water–gas shift.

In the context of power-to-X (PtX) technologies, [13] studied the flexible operation of renewable-powered PtX processes, assuming a linear process model, with additional energy buffers, a fuel cell and grid connections. However, this flexibility is achieved only through the use of various buffers and grid connections, while the production rate of the main PtX process remains constant. Ref. [14] explored the flexibility of PtX plants connected to a wind-farm by using a linearized process model. The electrolyser provides the greatest flexibility, whereas the PtX process allows deviations of only a few percent from the main operating point, leaving little of the feasible region covered. The flexible operation and configuration of the process chain allow the utilization of renewable energies. The flexibility of different sub-processes of PtX processes with a coupled proton exchange membrane (PEM) electrolyser is investigated in [15], demonstrating the suitability for flexible operation with renewable energy. Ref. [16] explored the optimal capacity and flexible operation of a power-to-ammonia process under fluctuating renewable energy supply by solving a two-stage algorithmic framework with particle swarm and MILP with a linear process model. The model consists of several steady-state operating conditions specified based on the literature, and the system can switch between them at set intervals. The annual profit can be increased while reducing carbon emissions. Ref. [17] examined the flexibility of a power-to-fuel plant and calculated the optimal hydrogen buffer size with historical wind and sun data. An electrolyser, a hydrogen storage, a battery and various hydrogen consuming PtX plants are considered in [18] to compute an optimal flexible schedule to reduce operation costs. For most of the PtX plants considered, a stationary operation is assumed, while one plant considers a linear model between power consumption and production capacity. Ref. [19] investigates the flexible operation of a power-to-ammonia plant with day-ahead electricity prices, using a simplified version of a complex dynamic process model. By optimizing operational parameters, the demand response potential can be increased.

Ref. [20] investigated the flexible operation of a PtM plant with a hydrogen storage and batteries. The scheduling problem, which assumes linearity for the process based on an Aspen Plus simulation model, solves for the optimal unit size and operation capacity of the plant, considering current and future time-variable electricity prices. The results show that especially the hydrogen storage is favorable. Ref. [21] optimized a PtM system, taking into account day-ahead electricity prices. The system includes buffer storages, an electrolyser and power from a wind turbine. The operational costs decreased by 4.5% utilizing the flexibility of different components of the system. However, a complex white-box modeling approach is used, which significantly increases the modeling effort. In [22], the operation of a PtM plant is optimized by analyzing the oversizing of process units, the consideration of intermediate storages and renewable power with a white-box modeling approach. The results show that flexible operation is feasible with an optimized design and intermediate storages. Ref. [23] developed a complex dynamic NARX model for a PtM process based on an Aspen Plus simulation model. The results show energy efficiencies of over 70% during dynamic operation. A PtM process coupled with a proton-conducting steam electrolyser is investigated in [24]. The developed dynamic white-box model shows high efficiencies depending on the process design and heat integration concept.

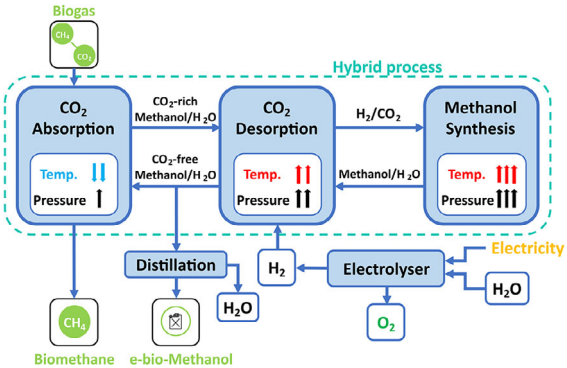

FIGURE 1 | Block flow diagram of the novel PtM process [27].

Current literature regarding the scheduling of PtX processes mostly uses complex white-box models, which are time-consuming and difficult to develop, or neglects possible nonlinearities and therefore does not reflect the complexity of the considered processes. It should also be noted that, in most cases, the main PtX process is operated only in a steady state at optimal capacity, and often allows for only limited flexibility covering just little of the feasible operating region.

Therefore, this work aims to develop a data-driven optimization framework using characteristic maps for optimal scheduling of the novel PtM process using decentralized CO_2 point sources, to exploit its flexibility. The contribution of the paper has the following aspects:

- Development of a data-driven optimization framework for the optimal scheduling of the PtM process using experimental and simulation data.
- Utilization of characteristic maps as process models instead of modeling physical equations, allowing for a much simpler creation of the framework with little prior knowledge while still taking any nonlinearities into account. This allows to represent complex processes like the PtM process considered.
- Simple adaptation of the characteristic maps to the respective process under consideration.
- Demonstration of the framework's effectiveness through 78 case studies focusing on cost minimization, emission reduction and self-sufficient operation for the considered PtM process.

This paper is structured as follows: Section 2 introduces the PtM process. Section 3 outlines the methodology, including data generation and the formulation of the optimization problem. Boundary conditions and case studies are described in Section 4, followed by a discussion of the results in Section 5. The paper concludes in Section 6 with a summary and outlook.

2 | Process Description

Figure 1 depicts the PtM process. The system consists of a carbon dioxide capture unit, a methanol synthesis, a distillation and an

TABLE 1 | Key performance indicators (KPI) of the different sub-processes of the PtM process.

Sub-process	Input	Output	KPI
CO_2-Capture	Biogas, MeOH–H_2O	CO_2-rich solvent	>99% CO_2-Capture
Methanol Synthesis	H_2, CO_2	MeOH–H_2O	77 Ld^{-1} yield
Distillation	MeOH–H_2O	MeOH	97% purity, 52 Ld^{-1} yield
Electrolyser	H_2O, electricity	H_2	99.9% purity, 4000 NLh^{-1} yield

electrolyser [25]. Biogas flows into the absorption column, where CO_2 is separated from methane using methanol–water as the absorption medium. The methanol–water mixture transports the dissolved CO_2 to the desorption column, where it is desorbed with hydrogen gas produced in an anion exchange membrane electrolyser (AEM). The low carbon dioxide methanol–water mixture flows back to the absorption unit, while the desorbed CO_2 mixes with the hydrogen and serves as synthesis gas. Under optimum operating conditions, over 99% of the CO_2 is absorbed and then desorbed (Table 1). The average energy consumption is around 10 kW. The CO_2 yield is approximately 72 kgd^{-1}. The synthesis gas flows through four consecutive plug flow reactors, where H_2 and CO_2 react to form a methanol–water mixture. The overall CO_2 conversion rate is about 80% with a yield of about 77 Ld^{-1}.

The resulting methanol–water mixture is used in the distillation, where the methanol is separated from the water to yield highly pure green methanol with roughly 97% purity and a yield of about 52 Ld^{-1}. The purity value is derived from simulations and measurement data from the pilot plant. The purified biogas is produced as a valuable by-product of the process. The total power consumption of the process is about 20 kW.

The electrolyser consists of eight modules, with each producing up to 500 NLh^{-1} hydrogen at up to 35 bar outlet pressure with a purity of 99.9%. The operative power consumption of all modules is 19.4 kW at maximum capacity [26].

To increase the flexibility of the process, additional buffer storage tanks are used. The hydrogen storage connects the electrolyser and the CO_2-Capture unit, while the methanol–water storage tank is located after the methanol synthesis and before the distillation. These intermediate storages, together with a modeled battery, allow for increased flexibility.

3 | Methodology

The data generation and model formulation are presented in the following section. Compared to [27], this work uses an extended scheduling model with improved consideration of the dynamics and new current data.

3.1 | Data Generation

The database for modeling and optimization is generated by simulations with the ASPEN Plus process engineering software [28]. The simulation model was developed based on the configuration of the pilot plant to ensure realistic representation of process performance. The absorption and desorption columns were modeled using rate-based RadFrac blocks with dimensions and internals consistent with the pilot plant design. The methanol synthesis section includes feed compression, a series of four plug flow reactors modeled using RPlug blocks and a multiphase separator represented by a Flash block. The compressor was modeled as a positive displacement unit. The distillation column for methanol purification was also simulated using a RadFrac block operating under equilibrium conditions, ensuring accurate representation of phase separation behavior.

Three different thermodynamic methods are used to model the process. The Perturbed chain-SAFT (PC-SAFT) is used in the CO_2 capture unit as it gives better solubility prediction compared to other equation of state models [29]. The Soave–Redlich–Kwong equation of state was selected due to its suitability for high-pressure methanol synthesis systems, where non-ideal gas behavior must be accounted for through fugacity corrections. It is widely used in literature and has been shown to provide results comparable to other cubic equations of state under typical operating conditions [30]. The non-random two-liquid (NRTL) model was employed for the distillation section due to its ability to accurately represent vapor–liquid equilibrium in non-ideal liquid mixtures such as methanol–water. Previous studies have shown that the NRTL model provides good agreement with experimental vapor–liquid experimental data for such systems [31]. The reaction kinetics for methanol synthesis and the reverse water–gas shift (RWGS) reaction were described using a Langmuir–Hinshelwood–Hougen–Watson (LHHW) model originally proposed by Vanden Bussche and Froment. The kinetic expressions and parameters used in this study were adopted from a modified formulation available in the literature, where the original model was rearranged to ensure compatibility with Aspen Plus [32].

The simulation was performed based on the following assumptions:

- Biogas is considered as the CO_2 source, with a composition of 35 mol% CO_2 and 65 mol% CH_4, and no additional impurities are included.
- Hydrogen is assumed to be 100% pure.
- All reactors are modeled under adiabatic conditions.
- Pressure drops in the absorption, desorption and distillation columns are calculated based on the hydraulic characteristics of the column internals.
- Pressure drops in the reactors are estimated using the Beggs–Brill correlation.
- Heat losses to the surroundings are neglected.
- Heat integration is implemented in accordance with the pilot plant configuration.

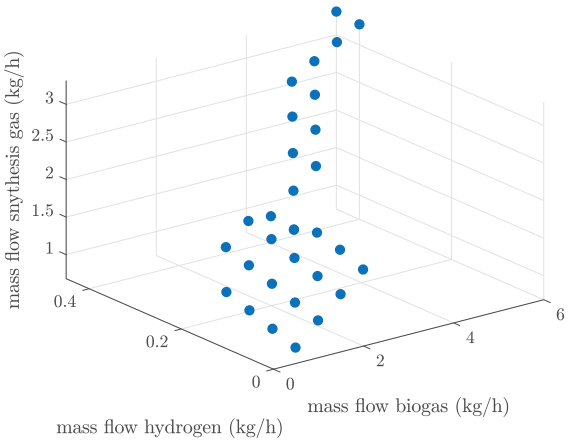

FIGURE 2 | Exemplary characteristic map of the CO_2-Capture unit and methanol synthesis unit with two independent variables.

In a first step, characteristic maps are created for each sub-process based on simulation data of the stationary operation of the PtM process. They describe the relationship between a dependent and one or more independent variables and consist of a certain number of operating points. These characteristic maps are used in many industrial areas, particularly in the engine, compressor and turbine industries [33, 34].

Independent and dependent variables are defined for each process unit to generate the characteristic maps. Although the process has three sub-processes, only two are considered here due to the coupling of the CO_2-Capture and methanol synthesis. For the characteristic maps of the first sub-process (CO_2-Capture and methanol synthesis), two independent variables (mass flow of hydrogen and biogas) and 10 dependent variables are defined. Figure 2 shows an exemplary characteristic map of the CO_2-Capture unit and methanol synthesis with the mass flow of synthesis gas as the dependent variable. Sub-process 2 (distillation) has one independent variable (mass flow of methanol–water) and five dependent variables. The dependent variables are the output mass flows of methane, methanol–water, synthesis gas, methanol and the power consumption of the plant components such as pumps, heaters and coolers, as well as the molar composition of individual process streams.

To determine the correlation between the dependent and independent variables, one stationary simulation is carried out for each operating point, which is defined by specific combinations of the independent variables. The first sub-process includes 31 operating points, while the second uses one independent variable with 10 operating points. The selection of the operating points is based on expert knowledge and the operation and operating range of the pilot plant of the considered PtM process. All operating points of one sub-process form its characteristic map.

The main advantage of using characteristic maps is their simplicity: They can be created from data from experiments or simulations of the PtM plant without complex physical modeling. Additionally, non-linearities can easily be incorporated. While characteristic maps do not capture the dynamics of the process, with the use of ramping constraints, the dynamic behavior can still be considered despite the use of stationary data.

3.2 | Mathematical Formulation

The scheduling of the process is formulated as an MINLP, enabling to capture discrete decisions (operating modes and points) and continuous variables. The formulation is according to [35] denoted as:

$$\begin{aligned} \underset{x}{\text{minimize}} \quad & f(x), \\ \text{subject to} \quad & g(x) \leq 0, \\ & x \in X, \quad x_i \in Z, \quad \forall i \in I. \end{aligned} \tag{1}$$

The constraints $g(x)$ and the objective function $f(x)$ will be described in the next passages.

3.2.1 | Constraints

The model includes constraints for operating modes and points, ramping and transitions for the dynamics, energy management and buffer storages, the battery and the electrolyser.

Operating mode In each time step, each sub-process can only be in one of five specific operating modes:

- Off
- Start up
- On
- Standby
- Shutdown

The binary variables $x^u_{t,m}$ indicate whether the unit u is operating in mode m at time step t. Since each sub-process has to be in exactly one operating mode, the sum of all operating modes per sub-process has to be equal to one at every time step:

$$\sum_{m \in \mathbb{M}} x^u_{t,m} = 1. \tag{2}$$

To model transitions between different operating modes, auxiliary variables $z^u_{t,m,m'}$ are introduced, which describe the switching from one mode m to another mode m', following [36]:

$$x^u_{t-1,m} \geq z^u_{t,m,m'}, \tag{3}$$

$$x^u_{t,m'} \geq z^u_{t,m,m'}, \tag{4}$$

$$x^u_{t-1,m} + x^u_{t,m'} - 1 \leq z^u_{t,m,m'}. \tag{5}$$

Furthermore, forbidden transitions are defined in order to avoid prohibited operating mode changes, for example, the switching from "Off" to "On." This is implemented with the following constraint:

$$z^u_{t,m,m'} \equiv 0. \tag{6}$$

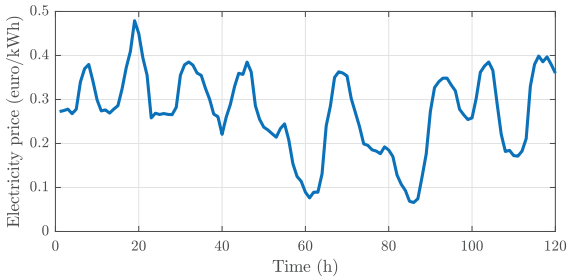

FIGURE 3 | Dynamic electricity price of an exemplary working week [41].

Here, m' are the operating modes that cannot be changed to from mode m. For example is $z^u_{t,Off,On} \equiv 0$, since no sub-process can directly change from mode "Off" to "On."

In addition, transitional constraints are defined, which describe that after a change from operating mode m to m', a change to another mode m'' is necessary:

$$z^u_{t,m,m'} = z^u_{t+\underline{T}^u_{m,m'},m',m''} \tag{7}$$

with $\underline{T}^u_{m,m'}$ equals the minimum time the sub-process u has to be in mode m' after a change from mode m before changing to mode m''.

Operating point For every time step, each of the sub-processes can also only operate in one discrete operating point. The binary variables $y^u_{t,o}$ for every time step t, operating point o and unit u are used for modeling. Since only one operating point can be active, the sum of all operating points per sub-process has to be equal to one at every time step:

$$\sum_{o\in\mathbb{O}} y^u_{t,o} = 1. \tag{8}$$

As not all operating points can be operated per operating mode, an additional constraint must be introduced.

$$x^u_{t,m} = \sum_{o\in\mathbb{OM}} y^u_{t,o}. \tag{9}$$

$\mathbb{OM}$ describes all permitted operating points o for operating mode m. The sum of permitted operating points must be one if the mode is active and zero if the mode is inactive.

Ramping and transition constraints To account for the dynamics of the process, ramping constraints are introduced to limit individual physical variables by restricting their change per time step. To model these restrictions, the following constraints are formulated:

$$|v^u_{t,var} - v^u_{t-1,var}| \le \overline{K}^u_{var}. \tag{10}$$

$v^u_{t,var}$ is any physical variable of sub-process u and $\overline{K}^u_{var}$ is the maximum change allowed between two time steps. The constraints prevent operating points of an operating mode from being changed too quickly.

TABLE 2 | Examined case studies of the PtM process with OBJ: Electricity costs (1–8) and OBJ: Carbon footprint (9–16).

Case #	Description	PV (kWp)	Battery (kWh)
1	Stationary operation	—	—
2	Stationary operation	100	—
3	Stationary operation	—	200
4	Stationary operation	100	200
5	Flexible operation	—	—
6	Flexible operation	100	—
7	Flexible operation	—	200
8	Flexible operation	100	200
9	Stationary operation	—	—
10	Stationary operation	100	—
11	Stationary operation	—	200
12	Stationary operation	100	200
13	Flexible operation	—	—
14	Flexible operation	100	—
15	Flexible operation	—	200
16	Flexible operation	100	200

Transition constraints describe the minimum and maximum time in which a sub-process can be operated after a change from mode m to mode m':

$$\sum_{\tau=t}^{\underline{T}^u_{m,m'}} x^u_{\tau,m'} \ge z^u_{t,m,m'} \cdot \underline{T}^u_{m,m'}, \tag{11}$$

$$1 - x^u_{t+\underline{T}^u_{m,m'},m'} \ge z^u_{t,m,m'} - \sum_{\tau=t+\underline{T}^u_{m,m'}}^{\overline{T}^u_{m,m'}} \sum_{(m,m')\in\mathbb{M}} z^u_{\tau,m,m'} \tag{12}$$

with $\underline{T}^u_{m,m'}$ equals the minimum time the sub-process u has to be in mode m' after a change from mode m and $\overline{T}^u_{m,m'}$ the maximum time. $\mathbb{M}$ includes all the permitted transitions from mode m to mode m'. These constraints ensure, for example, that a sub-process has to be in "Start up" mode for a certain time due to physical processes such as heating up.

Energy management The electricity can be purchased from the grid as well as generated by a photovoltaic system. The electricity from both sources can be stored in a battery. The power requirements of the system can then be covered directly from the grid, from the photovoltaic system and from the battery. This results in a power balance for each time step:

$$P^{batt,out}_t + P^{pv,used}_t + P^{grid}_t - P^{grid,batt}_t = P^{elec}_t + P^{plant}_t \tag{13}$$

Here $P^{batt,out}_t$ is the power taken from the battery, $P^{pv,used}_t$ is the power from the photovoltaic system used for the process, P^{grid}_t is the power bought from the grid, $P^{grid,batt}_t$ is the power from the grid which is stored in the battery and P^{elec}_t and P^{plant}_t is the power consumption of the electrolyser and plant, respectively.

The characteristic maps specify the power consumption and depend on the operating point and operating mode.

The electricity from the photovoltaic system can be stored in the battery and used directly for the process, which is limited by the amount of electricity produced by the photovoltaic system:

$$P_t^{pv,used} + P_t^{pv,batt} \leq P_t^{pv}. \tag{14}$$

For autonomous operation, electricity is not purchased from the grid, but is only supplied via the photovoltaic system and the battery:

$$P_t^{grid} = 0. \tag{15}$$

To ensure grid-friendly operation, the maximum power drawn from the grid can be capped:

$$P_t^{grid} \leq \overline{P}^{grid} \tag{16}$$

with $\overline{P}^{grid}$ being the maximum power purchased from the grid.

Battery The battery can be charged from the photovoltaic system and the power grid while providing power to the process and electrolyser. To prevent simultaneous charging and discharging, additional binary variables are introduced for charging (c_t^{pv} and c_t^{grid}) and discharging (dc_t^{out}). The following constraints prevent simultaneous charging and discharging:

$$c_t^{pv} + dc_t^{out} \leq 1, \tag{17}$$

$$c_t^{grid} + dc_t^{out} \leq 1. \tag{18}$$

Since the power from the photovoltaic system or the grid into the battery is either zero or a value between the minimum and maximum permitted charging power ($\underline{P}_c, \overline{P}_c$), additional variables are introduced. Z_t^{pv} and Z_t^{grid} describe the charging power of the battery and have a range from zero to the maximum charging power. The following constraints ensure that the actual charging power P_t^{pv} and P_t^{grid} is not between zero and $\underline{P}_c$:

$$P_t^{pv} = c_t^{pv} \cdot Z_t^{pv}, \tag{19}$$

$$P_t^{pv} \leq Z_t^{pv} - (1 - c_t^{pv}) \cdot \underline{P}_c, \tag{20}$$

$$P_t^{pv} \geq Z_t^{pv} - (1 - c_t^{pv}) \cdot \overline{P}_c. \tag{21}$$

The same applies to the charging power of the battery from the grid P_t^{grid} and the discharging power of the battery P_t^{out}. To ensure that the maximum charging capacity of the battery is not exceeded, the following additional constraint is introduced:

$$P_t^{pv} + P_t^{grid} \leq \overline{P}_c. \tag{22}$$

Finally, the state of charge (SOC) of the battery is calculated as follows:

$$SOC_t^{batt} = SOC_{t-1}^{batt} + \frac{(P_t^{grid,batt} + P_t^{pv,batt}) \cdot \eta^{charge,batt} - P_t^{batt,out}}{C^{batt}} \cdot 100. \tag{23}$$

SOC_t^{batt} is the state of charge, C^{batt} the capacity and $\eta^{charge,batt}$ the charging efficiency of the battery.

Storage constraints To ensure that the contents of the buffer storages or the battery do not exceed their limits, following constraints are introduced:

$$\underline{Pr}^{H_2} \leq Pr_t^{H_2} \leq \overline{Pr}^{H_2}, \tag{24}$$

$$\underline{F}^{MeOH-H_2O} \leq F_t^{MeOH-H_2O} \leq \overline{F}^{MeOH-H_2O}, \tag{25}$$

$$\underline{C}^{batt} \leq \frac{SOC_t^{batt}}{100} \cdot \overline{C}^{batt} \leq \overline{C}^{batt}. \tag{26}$$

$Pr_t^{H_2}$ is the pressure in the hydrogen storage tank, $\underline{Pr}^{H_2}$ and $\overline{Pr}^{H_2}$ the minimum and maximum allowed pressure in the hydrogen storage tank. $F_t^{MeOH-H_2O}$ is the filling level of the methanol–water storage tank and $\underline{F}^{MeOH-H_2O}$ and $\overline{F}^{MeOH-H_2O}$ the minimum and maximum allowed filling level of the storage. $\underline{C}^{batt}$ and $\overline{C}^{batt}$ is the minimum and maximum allowed capacity of the battery.

Electrolyser Each module of the electrolyser can be operated in four modes, namely "start up," "standby," "off" and "running," which are represented by the binary variables $su_{t,n}^{elec}$, $s_{t,n}^{elec}$, $o_{t,n}^{elec}$ and $r_{t,n}^{elec}$. The following constraints are formulated:

$$su_{t,n}^{elec} + s_{t,n}^{elec} + o_{t,n}^{elec} + r_{t,n}^{elec} = 1, \tag{27}$$

$$su_{t-1,n}^{elec} \leq r_{t,n}^{elec}, \tag{28}$$

$$s_{t-1,n}^{elec} \leq o_{t,n}^{elec} + r_{t,n}^{elec}, \tag{29}$$

$$o_{t-1,n}^{elec} \leq su_{t,n}^{elec} + o_{t,n}^{elec}, \tag{30}$$

$$r_{t,n}^{elec} \leq s_{t,n}^{elec} + o_{t,n}^{elec} + r_{t,n}^{elec}. \tag{31}$$

Equation (27) ensures that only one mode is active in every time step and for every electrolyser module. The constraints (28)–(31) describe the permitted transitions between the different modes.

3.2.2 | Objective Function

Depending on the scenario, different objective functions are used. The first objective function is the minimization of the electricity costs:

$$OBJ_{costs} = \min \sum_{t \in T} P_t^{grid} \cdot p_t^{electricity}. \tag{32}$$

Here $p_t^{electricity}$ is the dynamic electricity price and P_t^{grid} is the power consumption of all components at time t.

Alternatively, the carbon footprint can be minimized:

$$OBJ_{CO_2-footprint} = \min \sum_{t \in T} P_t^{grid} \cdot CI_t^{electricity}. \quad (33)$$

Here $CI_t^{electricity}$ is the carbon intensity of the purchased electricity, which will be explained in the following section.

In self-sufficient operation, no power from the grid can be purchased. Therefore, the objective is to maximize the amount of methanol that can be produced with only power from a photovoltaic system:

$$OBJ_{methanol} = \max \sum_{t \in T} M_t^{MeOH}, \quad (34)$$

M_t^{MeOH} is the amount of methanol produced at time t.

4 | Case Studies

This section outlines the boundary conditions and assumptions for the process optimization and describes the analyzed cases of the work. The following assumptions were made:

- **Benchmark cases**: Each unit u of the PtM process operates in a steady state in one single operating point o over the whole horizon (after the start up). This operating point is computed by systematically exploring all operating points and minimizing the costs. This leads to an already optimized but stationary operation. This is ensured by additional constraints:

$$y_{t-1,o}^u = y_{t,o}^u. \quad (35)$$

- **Initial and final conditions**: The storage fill levels and the battery charge must be similar at the beginning and end of the horizon, with a tolerance of 5%:

$$| P_0^{H_2} - P_T^{H_2} | \leq P_{tol}^{H_2}, \quad (36)$$

$$| F_0^{MeOH-H_2O} - F_T^{MeOH-H_2O} | \leq F_{tol}^{MeOH-H_2O}, \quad (37)$$

$$| SOC_0^{batt} - SOC_T^{batt} | \leq SOC_{tol}^{batt}. \quad (38)$$

- **Methanol production target**: A fixed amount of methanol (108 kg ± 1%) must be produced within the horizon when minimizing the electricity costs or the CO_2 footprint. This corresponds to 75% production capacity.
- **Process dynamics**: The associated data for the ramping and transition constraints come from a test campaign of the PtM pilot plant. The dynamics are mainly caused by slow heating and cooling processes. This includes times for start-up of the different process units and also the power consumption during start-up, standby and shutdown operating mode. For example, the methanol synthesis start-up takes about 12 h, CO_2 capture takes about 6 h and distillation also takes 6 h. The standby and start-up power of the pilot plant is measured as a percentage of power consumption at 100% capacity and then adjusted to match the power consumption at 100% capacity of the simulation data. The dynamics of the electrolyser are in the minute range and are therefore not considered due to the hourly time step.

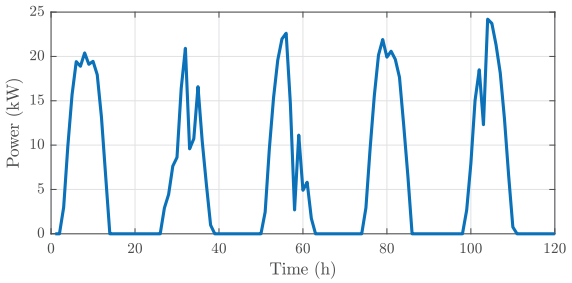

FIGURE 4 | Generated photovoltaic power for an exemplary working week.

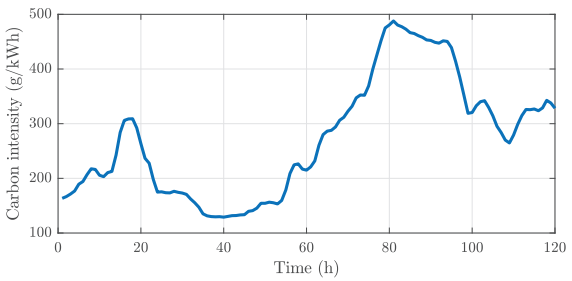

FIGURE 5 | Calculated carbon intensity of the German electricity production for an exemplary working week [39].

- **Electricity prices**: Dynamic prices, based on 2023 historical data for typical working weeks (Monday to Friday), are used (Figure 3).
- **Photovoltaic system**: A photovoltaic system using the python "pvlib" toolbox [37] is considered, simulating electricity generation with perfect weather forecast data from [38] (Figure 4). To adjust the output of the photovoltaic system, the peak power generation is scaled to the considered sizes with a peak power of 100, 200, 300, 400 and 500 kW.
- **Battery**: Capacities of 200, 400, 600, 800 and 1000 kWh are considered. For all battery sizes, the overall efficiency is considered to be 90%.
- **Carbon footprint minimization**: Instead of just minimizing the electricity costs of the process, it is also possible to minimize the carbon dioxide footprint. Carbon intensity is used to measure the carbon footprint of the electricity production. It describes the amount of grams of CO_2 per kWh of electricity produced and is calculated based on emission factors of individual electricity sources and their share in the current electricity mix [39]. Historical data of the German electricity production from the year 2023 are used (Figure 5).
- **Optimization setup**:
  - Fifty-two optimizations are carried out for all working weeks (Monday to Friday) of 1 year. The results are then averaged.

TABLE 3 | Examined case studies of the self-sufficient operation of the PtM process (Cases 17–66) with OBJ: Production volume.

Case #	Description	PV (kWp)	Battery (kWh)
17–21	Stationary operation	100	200, 400, 600, 800, 1000
22–26	Stationary operation	200	200, 400, 600, 800, 1000
27–31	Stationary operation	300	200, 400, 600, 800, 1000
32–36	Stationary operation	400	200, 400, 600, 800, 1000
37–41	Stationary operation	500	200, 400, 600, 800, 1000
42–46	Flexible operation	100	200, 400, 600, 800, 1000
47–51	Flexible operation	200	200, 400, 600, 800, 1000
52–56	Flexible operation	300	200, 400, 600, 800, 1000
57–61	Flexible operation	400	200, 400, 600, 800, 1000
62–66	Flexible operation	500	200, 400, 600, 800, 1000

TABLE 4 | Examined case studies of the PtM process (Cases 67–70) with OBJ: production volume.

Case #	Description	PV (kWp)	Battery (kWh)
67	Flexible operation	2914	4582
68	Stationary operation	2914	4582
69	Stationary operation	4288	5615
70	Flexible operation	4288	5615

TABLE 5 | Examined case studies of the PtM process (Cases 71–78) for peak load capping.

Case #	Description	Objective	Max. load (%)
71	Stationary operation	Electricity costs	80
72	Stationary operation	Electricity costs	90
73	Stationary operation	Carbon footprint	80
74	Stationary operation	Carbon footprint	90
75	Flexible operation	Electricity costs	80
76	Flexible operation	Electricity costs	90
77	Flexible operation	Carbon footprint	80
78	Flexible operation	Carbon footprint	90

- The optimization horizon is 120 h with a 1-h time step. This choice is based on a trade-off between computation time, electricity price forecast accuracy and optimization potential, since computation time increases as the horizon lengthens, forecast accuracy decreases and optimization potential improves.
- The MINLP is solved using GUROBI [40] with a 1000 s time limit and 1% optimality gap.

Cases 1–16 evaluate electricity costs and carbon footprint minimization. Cases 17–66 explore the self-sufficient operation under various photovoltaic system and battery sizes, while Cases 67–70 consider the self-sufficient operation with optimized sizing. Cases 71–78 implement peak load capping.

Table 2 shows the cases with the minimization of the electricity costs (Cases 1–8) and the CO_2 footprint (Cases 9–16) as the objective function. Scenarios 17 to 66 (Table 3) consider the self-sufficient operation of the PtM process without purchasing electricity from the grid using only power from the modeled photovoltaic system. Since the operation with just a photovoltaic system would result in the shutdown of the process every night, a battery is also considered to ensure continuous operation. Combinations of five photovoltaic system sizes and five battery sizes are considered.

In Case 67 (Table 4), the size of the photovoltaic system and the battery is optimized for the self-sufficient flexible operation, so that at least 90% of working weeks reach a minimum production capacity of 75%. As optimization over the entire year is not possible due to the long time horizon, the optimum photovoltaic system and battery size is calculated individually for each working week and the worst 10% of weeks (requiring the largest photovoltaic system and battery size) are excluded. From the remaining 90%, the maximum size of the photovoltaic system and battery is selected and used in Case 67 for all weeks. The same photovoltaic system and battery size are then used for Case 68 for the stationary operation. In Case 69, the battery size and photovoltaic system size are optimized again with the same principle as for Case 67, but for stationary operation. This is then compared to the production capacity of Case 70, where the flexible operation of the process with the same photovoltaic system and battery configuration is regarded. Since the battery size tends to be very large, the tolerance for initial and final charge equality of the battery is set to an absolute value of 50 kWh.

Cases 71–78 (Table 5) include peak load capping, with two different maximal power inputs allowed and different objective functions (electricity costs and carbon footprint). No photovoltaic system or battery is considered here.

5 | Results and Discussion

Flexible operation consistently outperformed stationary baselines. In electricity cost minimization scenarios, up to 31% cost savings were achieved. The CO_2 footprint was reduced by up to 24% and in self-sufficient setups, flexible operation enabled a 14.5 times higher methanol yield on average using the same photovoltaic system and battery setup.

First, the results for the Cases 1–16 are discussed. The self-sufficient operation of the PtM process is then covered, before

TABLE 6 | Results of the examined case studies of the PtM process (Cases 1–16).

Case #	Description	PV (kWp)	Battery (kWh)	Elec. costs (€)	CO_2 footprint (kg)	Prod. vol. (kg)	Comp. time (s)	Opt. gap (%)
1	Stationary	—	—	526.87	1734.84	108.07	0.60	0.00
2	Stationary	100	—	451.61	1504.61	108.07	0.62	0.00
3	Stationary	—	200	481.79	1764.30	108.07	1.28	0.00
4	Stationary	100	200	383.98	1437.00	108.07	1.36	0.00
5	Flexible	—	—	416.77	1414.19	108.09	84.16	0.00
6	Flexible	100	—	341.94	1179.14	108.09	142.05	0.00
7	Flexible	—	200	377.46	1428.61	108.09	93.09	0.00
8	Flexible	100	200	286.22	1112.88	108.09	88.99	0.00
9	Stationary	—	—	526.87	1734.84	108.07	0.74	0.00
10	Stationary	100		451.61	1504.61	108.07	0.73	0.00
11	Stationary	—	200	511.82	1688.47	108.07	0.98	0.00
12	Stationary	100	200	411.84	1377.44	108.07	1.41	0.18
13	Flexible	—	—	426.76	1387.72	108.09	256.04	0.00
14	Flexible	100	—	352.06	1160.46	108.09	85.72	0.00
15	Flexible	—	200	411.11	1345.27	108.09	95.53	0.00
16	Flexible	100	200	315.74	1048.74	108.09	97.74	0.00

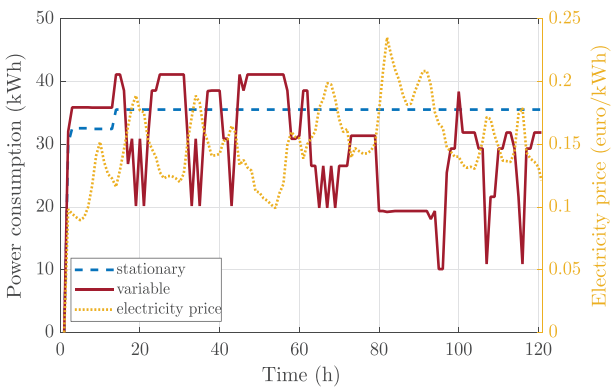

FIGURE 6 | Power consumption and electricity price of the flexible operation (Case 5) compared to the stationary operation (Case 1) for an exemplary working week.

operation with peak load capping is considered. Stationary operation is always compared to flexible operation.

The results for the Cases 1–16 are shown in Table 6. Comparing Case 1 (stationary operation) with Case 5 (flexible operation), an average cost reduction of over 20% is achieved. Figure 6 shows the power consumption of the process and the electrolyser as well as the electricity price for an exemplary working week. In the stationary case, the process is operated in one operating point after the start up (around hour 15). In contrast, in the flexible case, the power consumption adjusts depending on the electricity price, reducing the production capacity during high prices and increasing the capacity during low prices to meet the methanol demand. While the distillation operates at just one operating point (Figure 7), the CO_2-Capture unit and the methanol synthesis switch mostly between two operating points. The electrolyser

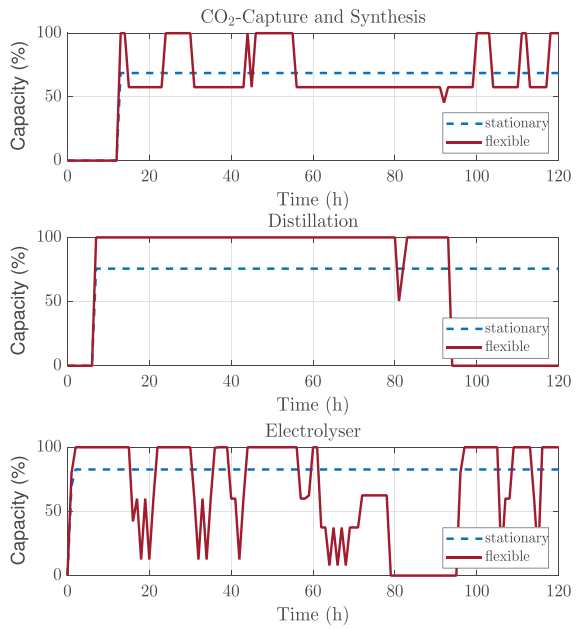

FIGURE 7 | Capacity of the different sub-processes of the flexible operation (Case 5) compared to the stationary operation (Case 1) for an exemplary working week.

shows the highest flexibility, where the production capacity and thus the electricity consumption change considerably over time. The SOC of the hydrogen and methanol–water storage tanks is shown in Figure 8. In the flexible operation, the hydrogen storage is fully utilized, enabling storage during low-price periods and usage during high-price periods. For the methanol–water storage, both the flexible and stationary operation utilize just a small part of the storage.

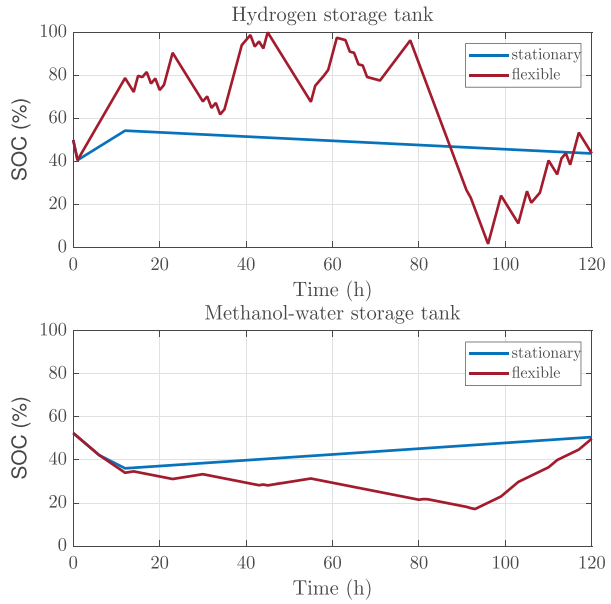

FIGURE 8 | SOC of the hydrogen and methanol–water storage tanks of the flexible operation (Case 5) compared to the stationary operation (Case 1) for an exemplary working week.

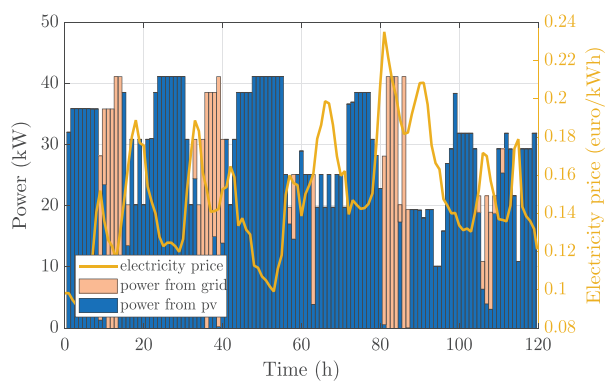

FIGURE 9 | Power consumption of the process, divided into power from the photovoltaic system and from the grid for the flexible operation (Case 6) for an exemplary working week.

With a photovoltaic system of 100 kWp, nearly 25% of costs can be saved comparing the flexible (Case 6) with the stationary operation (Case 2). Figure 9 illustrates the power consumption for the flexible operation. Especially in times of high electricity prices, the power consumption is lowered to avoid high electricity costs. In addition, the peak energy consumption occurs when sufficient electricity is provided by the photovoltaic system or when electricity prices are low.

Considering a battery with a capacity of 200 kWh, an average cost reduction of around 21% is possible, comparing the stationary (Case 3) with the flexible operation (Case 7), which is just 1 pp higher than without a battery. Accordingly, in this case, a battery alone does not contribute significantly to flexibility and lower electricity costs. With both a photovoltaic system and a battery, the average cost reduction is 31%, which is an additional 7 pp higher than with just a photovoltaic system and 10 pp higher than with just a battery.

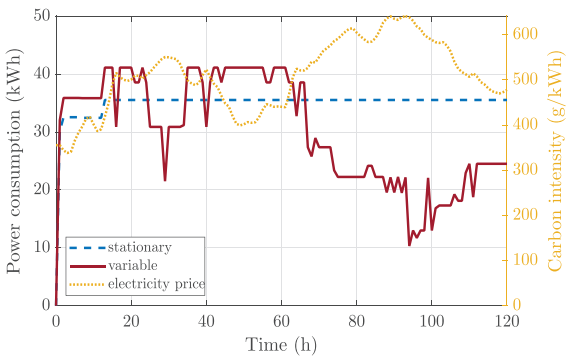

FIGURE 10 | Power consumption and carbon intensity of the flexible operation (Case 13) compared to the stationary operation (Case 9) for an exemplary working week.

A carbon footprint reduction of over 20% is possible when comparing the stationary (Case 9) with the flexible operation (Case 13), while electricity costs also decreased by 19%. Figure 10 shows the power consumption and the carbon intensity for an exemplary working week. The power consumption of the flexible operation increases in times of a low carbon intensity (first 60 h), while it decreases when the carbon intensity is high. Minimizing the CO_2 footprint also reduces electricity costs due to the correlation between the electricity price and carbon intensity. Prices are low when renewable energy sources like photovoltaics and wind dominate the energy mix, since they have a very low carbon intensity compared to conventional fossil energy sources.

If a photovoltaic system is considered, the reduction of the carbon footprint is nearly 23% comparing the stationary (Case 10) to the flexible operation (Case 14), while in case of a battery (Case 11 and Case 15), the reduction of a little over 20% is nearly the same as without a battery. Using both a photovoltaic system and a battery, the reduction of the carbon footprint is nearly 24%. These results confirm that flexible operation also reduces the carbon footprint.

Table 7 shows the results of the Cases 17–66 with autonomous operation. Since no electricity is drawn from the grid, the objective is to maximize the amount of methanol. Five different photovoltaic system sizes and five different battery sizes for each the stationary and flexible operation are considered. As no weekly production volume of methanol is specified for these cases, the total production volume over a year (annual production) is considered here (column 5 in Table 7).

In stationary operation, all the working weeks for most cases have an infeasible solution. There is not enough electricity with the considered photovoltaic system and battery to run the process stationary over 120 h. The reason for the infeasible weeks in steady-state operation is that, under these stationary conditions, it is not permitted to shut down the plant or change the operating point (see Equation (35)). This constraint ensures that the plant must remain in continuous operation in the same operating point. If there is not enough electricity available to operate the plant, the problem becomes therefore infeasible. In just 12 cases, there are a few weeks where a stationary operation is possible. In Case 24, stationary operation would only be possible in a single week of the year. The annual produced amount of methanol is between 72.05 kg and 648.41 kg, which corresponds to an annual utilization

TABLE 7 | Results of the examined case studies of the PtM process (Cases 17–66) for self-sufficient operation.

Case #	Description	PV (kWp)	Battery (kWh)	Annual prod. (kg)	Comp. time (s)	Opt. gap (%)	# Inf. weeks	# weeks no solution after 1000 s
17	Stationary	100	200	—	—	Inf	52	0
18	Stationary	100	400	—	—	Inf	52	0
19	Stationary	100	600	—	—	Inf	52	0
20	Stationary	100	800	—	—	Inf	52	0
21	Stationary	100	1000	—	—	Inf	52	0
22	Stationary	200	200	—	—	Inf	52	0
23	Stationary	200	400	—	—	Inf	52	0
24	Stationary	200	600	72.05	0.51	0	51	0
25	Stationary	200	800	72.05	0.55	0	51	0
26	Stationary	200	1000	144.10	0.36	0	50	0
27	Stationary	300	200	—	—	Inf	52	0
28	Stationary	300	400	—	—	Inf	52	0
29	Stationary	300	600	72.05	0.55	0	51	0
30	Stationary	300	800	180.12	0.53	0	50	0
31	Stationary	300	1000	324.22	0.74	0	48	0
32	Stationary	400	200	—	—	Inf	52	0
33	Stationary	400	400	—	—	Inf	52	0
34	Stationary	400	600	288.20	1.16	0	48	0
35	Stationary	400	800	324.22	0.80	0	48	0
36	Stationary	400	1000	540.35	1.87	0	46	0
37	Stationary	500	200	—	—	Inf	52	0
38	Stationary	500	400	—	—	Inf	52	0
39	Stationary	500	600	288.20	0.65	0	48	0
40	Stationary	500	800	648.41	0.56	0	45	0
41	Stationary	500	1000	648.41	0.50	0	45	0
42	Flexible	100	200	531.05	734.23	1.01	0	7
43	Flexible	100	400	604.32	789.68	1.09	0	12
44	Flexible	100	600	579.57	764.14	1.46	0	12
45	Flexible	100	800	616.97	846.98	0.92	0	13
46	Flexible	100	1000	590.23	824.74	1.37	0	15
47	Flexible	200	200	994.86	833.65	0.35	0	0
48	Flexible	200	400	1464.03	712.18	0.40	0	1
49	Flexible	200	600	1747.34	752.12	0.58	0	0
50	Flexible	200	800	1716.35	691.47	0.75	0	0
51	Flexible	200	1000	1807.23	750.41	0.60	0	0
52	Flexible	300	200	1218.42	820.36	0.23	0	1
53	Flexible	300	400	2004.44	748.58	0.12	0	2
54	Flexible	300	600	2334.15	612.35	0.12	0	1
55	Flexible	300	800	2597.15	654.49	0.14	0	2
56	Flexible	300	1000	2601.00	608.67	0.13	0	2

(Continues)

TABLE 7 | (Continued)

Case #	Description	PV (kWp)	Battery (kWh)	Annual prod. (kg)	Comp. time (s)	Opt. gap (%)	# Inf. weeks	# weeks no solution after 1000 s
57	Flexible	400	200	1359.16	820.32	0.80	0	0
58	Flexible	400	400	2317.67	853.80	0.33	0	3
59	Flexible	400	600	2778.81	482.90	0.16	0	2
60	Flexible	400	800	3128.47	715.10	0.21	0	3
61	Flexible	400	1000	3270.85	538.00	0.16	0	3
62	Flexible	500	200	1455.40	849.19	0.15	0	0
63	Flexible	500	400	2568.45	683.40	0.24	0	2
64	Flexible	500	600	3133.99	438.57	0.78	0	2
65	Flexible	500	800	3548.76	448.42	0.15	0	2
66	Flexible	500	1000	3640.38	363.24	0.25	0	2

TABLE 8 | Results of the examined case studies of the PtM process (Cases 67–70) for self-sufficient operation.

Case #	Description	PV (kWp)	Battery (kWh)	Prod. vol. (kg)	Comp. time (s)	Opt. gap (%)	# Inf. weeks	# weeks capacity < 75%
67	Flexible	2914	4582	139.07	14.55	0	0	5
68	Stationary	2914	4582	108.07	0.24	0	6	8
69	Stationary	4288	5615	108.07	0.57	0	3	5
70	Flexible	4288	5615	139.31	36.44	0	0	3

of only between 1% and 9%. With these photovoltaic system and the battery sizes, the process would be at a standstill most of the time. A significantly larger photovoltaic system and battery would be required to ensure continuous stationary operation.

In flexible operation, there are no infeasible weeks, since the constraint from Equation (35) is not active. The process therefore can be shutdown or change its operating point when no sufficient power is supplied. However, in some configurations, the optimization of some weeks was not completed within the specified computing time and no result is available. The annual production volume of methanol increases, the larger the photovoltaic system and the battery. In the smallest configuration (Case 42), the annual production is 531.05 kg (8.5% capacity), while in the largest configuration (Case 66), it reaches 51%. The amount of methanol produced with flexible operation is on average 14.5 times higher when compared to stationary operation, where at least the operation of 1 week is feasible. The key advantage of flexible operation is the possibility to operate all year round and with a much higher annual production rate, while with the stationary operation, the capacity utilization is much smaller.

Table 8 shows the self-sufficient Cases 67–70. The used photovoltaic system and battery sizes are calculated so that in at least 90% of weeks the production capacity is at least 75% (4). For Case 67, only 5 weeks have a production capacity less than 75%. With the same configuration, the stationary operation (Case 68) has 8 weeks with too little capacity, of which six are not feasible at all. In addition, the amount of methanol produced in flexible operation is almost 29% higher than in stationary operation.

For Case 69, the photovoltaic system and battery sizes are computed, so that the production capacity for the stationary operation is at least 75% for 90% of weeks. This leads to greater sizes compared to Case 67. Comparing the flexible (Case 70) to the stationary operation (Case 69), the production volume of methanol is nearly 29% higher. Also, there are fewer weeks with a capacity less than 75%, respectively, three for the flexible and five for the stationary operation.

The last cases (Table 9) considered are about peak load capping. The maximum electricity consumption of the process is limited to 80% and 90% of the maximum power consumption.

When the maximum power is capped at 80%, the methanol production for the stationary operation (Case 71) decreases to 72,05 kg per week, resulting in a capacity of roughly 50%. This is because the optimum operating point has a power consumption greater than 80% of the maximum power consumption, resulting in a suboptimal operating point for stationary operation. Comparing the stationary with the flexible operation (Case 75), an average decrease of nearly 35% of the electricity costs is achieved.

TABLE 9 | Results of the examined case studies of the PtM process (Cases 71–78) with peak load capping.

Case #	Description	Objective	Max. load (%)	Elec. costs (€)	CO_2 footprint (kg)	Prod. vol. (kg)	Comp. time (s)	Opt. gap (%)
71	Stationary	Elec. costs	80%	412.53	1358.39	72.05	0.33	0
72	Stationary	Elec. costs	90%	526.87	1734.84	108.07	0.33	0
73	Stationary	CO_2 footprint	80%	412.53	1358.39	72.05	0.34	0
74	Stationary	CO_2 footprint	90%	526.87	1734.84	108.07	0.33	0
75	Flexible	Elec. costs	80%	270.50	924.91	72.06	331.85	0
76	Flexible	Elec. costs	90%	422.34	1425.96	108.09	150.39	0
77	Flexible	CO_2 footprint	80%	278.87	903.59	72.06	414.01	0
78	Flexible	CO_2 footprint	90%	430.85	1402.68	108.09	181.66	0

When the allowed peak load is 90% of the maximum power consumption, the cost reduction is about 20%, comparing the stationary (Case 72) with the flexible operation (Case 76). With a lower maximum permitted peak power consumption, more costs can therefore be saved through flexible operation, although less methanol is produced. When minimizing the carbon footprint, flexible operation achieves a reduction of 33% for 80% peak load and 19% for 90% peak load compared to stationary operation. When the maximum power consumption is limited, not only can the electricity costs and the carbon footprint be reduced, but also the production volume of methanol can be increased due to flexible operation.

In practice, the power consumption is often limited only for short time periods and not the whole optimization time. This allows the target amount of methanol to be produced through flexible operation by increasing production capacity at other times, whereas this is not possible under steady-state operation (see Table 9, Case 71 compared to Case 72).

6 | Conclusion

This paper investigates the optimal flexible operation of a PtM process by performing an optimization concerning electricity price, CO_2 footprint and optimal self-sufficient operation using a photovoltaic system. The formulation as an MINLP and the solution of the optimization problem lead to a cost reduction of up to 31% due to the optimized flexible operation of the process in the case of a dynamic electricity price. Adding a photovoltaic system or a battery can further enhance the flexibility potential of the process. The CO_2 footprint is reduced by up to 24%.

The self-sufficient operation of the PtM process is possible, depending on the photovoltaic system and battery size. In flexible operation, on average 14.5 times more methanol is produced compared to stationary operation. Only with the flexible operation is it possible the operate the process all year round when considering the self-sufficient operation of the PtM process. If the same quantity is produced in both stationary and flexible operation, a significantly smaller photovoltaic system (32%) and battery (18.5%) are required for flexible operation. The PtM process can also be used to stabilize the electricity grid by reducing the peak electricity consumption, whereby the flexible operation leads to a reduction of electricity costs and the CO_2 footprint.

PtX technologies, particularly PtM, represent an important building block in the energy transition, enabling surplus renewable energy from the power grid to be used and at the same time producing green methanol as a climate-neutral fuel.

Important aspects for the future are the validation of the scheduling on the real process in order to test the flexible operation on a real system by constantly updating the schedule (e.g., every 24 h) to maintain a control loop.

Further extensions of the framework are important, like the adaptation of the process model during operation, which plays a major role due to changing operating characteristics because of wear and aging. This allows the limitation of the application due to model mismatch to be eliminated by continuously adapting the characteristic maps and dynamic constraints with new measurement data.

Furthermore, the approximation of the process dynamics must be validated by applying the calculated schedules to the pilot plant or a dynamic simulation model.

In addition, the simultaneous optimization of multiple objectives is an interesting aspect for future studies.

Ultimately, the applicability of the framework in a real environment plays a decisive role, which will be investigated in further studies by using real experimental data and testing the methodology on the real process.

Nomenclature

Symbols

c	binary variable for battery charging, –
C	battery capacity, kWh
CI	carbon intensity of electricity, $gkWh^{-1}$
dc	binary variable for battery discharging, –
F	filling level, m^3
$\overline{K}$	maximum change of a process variable, –
M	mass, kg

o	binary variable for mode off of the electrolyser, –
p	electricity price, euro/kWh
P	power, kW
$\underline{P}_c$	minimal power, kW
$\overline{P}_c$	maximal power, kW
Pr	pressure, bar
$\underline{Pr}_c$	minimal pressure, bar
$\overline{Pr}_c$	maximal pressure, bar
r	binary variable for mode running of the electrolyser, –
SOC	state of charge, –
s	binary variable for the standby of the electrolyser, –
su	binary variable for the start up of the electrolyser, –
$\underline{T}$	minimum stay time in one mode, h
$\overline{T}$	maximum stay time in one mode, h
v	placeholder for physical variables of the process, –
x	binary variable for the process operating mode, –
y	binary variable for the process operating point, –
z	binary variable for the change of the operating mode, –
Z	actual power, kW

Sub- and Superscripts

$batt$	battery
$elec$	electrolyser
$grid$	power grid
m	operating mode
o	operating point
pv	photovoltaic system
t	time step
u	process unit
var	process variable

Acknowledgments

This work is funded by the European Union. Views and opinions expressed are however those of the author(s) only and do not necessarily reflect those of the European Union or, neither the European Union nor the granting authority can be held responsible for them. This project has received funding from the European Union's Horizon Europe research and innovation programme under Grant Agreement No. 101083323.

Open access funding enabled and organized by Projekt DEAL.

Conflicts of Interest

The authors declare no conflicts of interest.

Data Availability Statement

The data that support the findings of this study are available from the corresponding author upon reasonable request.

References

1. A. Santecchia, I. Kantor, R. Castro-Amoedo, and F. Maréchal, "Industrial Flexibility as Demand Side Response for Electrical Grid Stability," *Frontiers in Energy Research* 10 (2022): 831462.

2. J. Ott, V. Gronemann, F. Pontzen, et al., "Methanol," in *Ullmann's Encyclopedia of Industrial Chemistry*, 1st ed. (Wiley-VCH, Ed. Wiley, 2012).

3. S. S. Tabibian and M. Sharifzadeh, "Statistical and Analytical Investigation of Methanol Applications, Production Technologies, Value-Chain and Economy With a Special Focus on Renewable Methanol," *Renewable and Sustainable Energy Reviews* 179 (2023): 113281.

4. L. C. Brée, K. Perrey, A. Bulan, and A. Mitsos, "Demand Side Management and Operational Mode Switching in Chlorine Production," *AIChE Journal* 65 (2019): e16352.

5. K. Roh, L. C. Brée, K. Perrey, A. Bulan, and A. Mitsos, "Flexible Operation of Switchable Chlor-Alkali Electrolysis for Demand Side Management," *Applied Energy* 255 (2019): 113880.

6. J. I. Otashu and M. Baldea, "Demand Response-Oriented Dynamic Modeling and Operational Optimization of Membrane-Based Chlor-alkali Plants," *Computers & Chemical Engineering* 121 (2019): 396–408.

7. A. Boldrini, D. Koolen, W. Crijns-Graus, E. Worrell, and M. Van Den Broek, "Flexibility Options in a Decarbonising Iron and Steel Industry," *Renewable and Sustainable Energy Reviews* 189 (2024): 113988.

8. X.-Y. Ye, Z.-W. Liu, M. Chi, M.-F. Ge, and Z. Xi, "Demand Response Optimization of Cement Manufacturing Industry Based on Reinforcement Learning Algorithm," in *2022 IEEE International Conference on Cyborg and Bionic Systems (CBS)* (IEEE, 2023), 402–406.

9. S. Siahchehre Kholerdi and A. Ghasemi-Marzbali, "Effect of Demand Response Programs on Industrial Specific Energy Consumption: Study at Three Cement Plants," *International Transactions on Electrical Energy Systems* 2022 (2022): 1–15.

10. M. T. Kelley, R. Baldick, and M. Baldea, "Demand Response Scheduling Under Uncertainty Chance-Constrained Framework and Application to an air separation unit," *AlChE Journal* (2020).

11. M. T. Kelley, R. Baldick, and M. Baldea, "Demand Response Operation of Electricity-Intensive Chemical Processes for Reduced Greenhouse Gas Emissions: Application to an Air Separation Unit," *ACS Sustainable Chemistry & Engineering* 7 (2019): 1909–1922.

12. M. T. Kelley, C. Tsay, Y. Cao, Y. Wang, J. Flores-Cerrillo, and M. Baldea, "A Data-Driven Linear Formulation of the Optimal Demand Response Scheduling Problem for an Industrial Air Separation Unit," *Chemical Engineering Science* 252 (2022): 117468.

13. M. Qi, D. N. Vo, H. Yu, et al., "Strategies for Flexible Operation of Power-to-X Processes Coupled With Renewables," *Renewable and Sustainable Energy Reviews* 179 (2023): 113282.

14. N. Moessner, P. Haebig, and K. Hufendiek, "Developing a Modelling-Approach to Represent Flexibility in Process Engineering—Implementation of a Dynamic Scheduling for a Green Power-to-X Production," *Procedia CIRP* 126 (2024): 508–512.

15. S. Mucci, A. Mitsos, and D. Bongartz, "Power-to-X Processes Based on PEM Water Electrolyzers: A Review of Process Integration and Flexible Operation," *Computers & Chemical Engineering* 175 (2023): 108260.

16. J. Zhou, Z. Zhang, R. Zhang, W. Zhang, G. Xu, and H. Wang, "Optimal Capacity and Multi-Stable Flexible Operation Strategy of Green Ammonia Systems: Adapting to Fluctuations in Renewable Energy," *Energy Conversion and Management* 314 (2024): 118720.

17. P. Pfeifer, L. Biffar, F. Timm, and T. Böltken, "Influence of Power-to-Fuel Plant Flexibility Towards Power and Plant Utilization and Intermediate Hydrogen Buffer Size," *Chemie Ingenieur Technik* 92 (2020): 1976–1982, https://onlinelibrary.wiley.com/doi/pdf/10.1002/cite.202000084.

18. S. Klyapovskiy, Y. Zheng, S. You, and H. W. Bindner, "Optimal Operation of the Hydrogen-based Energy Management System With P2X Demand Response and Ammonia Plant," *Applied Energy* 304 (2021): 117559.

19. T. Hochhaus, B. Bruns, M. Grünewald, and J. Riese, "Optimal Scheduling of a Large-Scale Power-to-Ammonia Process: Effects of Parameter Optimization on the Indirect Demand Response Potential," *Computers & Chemical Engineering* 170 (2023): 108132.

20. S. Mucci, A. Mitsos, and D. Bongartz, "Cost-Optimal Power-to-Methanol: Flexible Operation or Intermediate Storage?" *Journal of Energy Storage* 72 (2023): 108614–108614. ARXIV_ID: 2305.18338 MAG ID: 4385976730 S2ID:09912d3a44c03e1cb5738acfec306e65b8a4f38b.

21. Y. Zheng, S. You, X. Li, H. W. Bindner, and M. Münster, "Data-Driven Robust Optimization for Optimal Scheduling of Power to Methanol," *Energy Conversion and Management* 256 (2022): 115338.

22. C. Chen and A. Yang, "Power-to-methanol: The Role of Process Flexibility in the Integration of Variable Renewable Energy Into Chemical Production," *Energy Conversion and Management* 228 (2021): 113673.

23. X. Cui, S. K. Kær, and M. P. Nielsen, "Energy Analysis and Surrogate Modeling for the Green Methanol Production Under Dynamic Operating Conditions," *Fuel* 307 (2022): 121924.

24. S. Fogel, S. Unger, and U. Hampel, "Dynamic System Modeling and Simulation of a Power-to-Methanol Process Based on Proton-conducting Tubular Solid Oxide Cells," *Energy Conversion and Management* 300 (2024): 117970.

25. F. Vidal-Vazquez, R. Dittmeyer, and P. Pfeifer, "Vorrichtung und Verfahren zur Herstellung von Methanol aus Kohlendioxid," German Patent DE 10 2020 120 879 A1, Oct. 2022.

26. Enapter, "AEM Electrolyser EL4.1," (2024).

27. M. Kollmer, M. Vogelbacher, M. Terzi, M. Singh, F. Vidal-Vazquez, and J. Matthes, "Demand Response for a Novel Decentralized Power-To-Methanol Process," in *2024 International Conference on Smart Energy Systems and Technologies (SEST)* (IEEE, 2024), 1–6.

28. AspenTech, "Aspen Plus | Leading Process Simulation Software | AspenTech," (2025), https://www.aspentech.com/en/products/engineering/aspen-plus.

29. S. F. Baygi, "Application of the Perturbed Chain-SAFT Equation of State for Modeling CO2 Solubility in Aqueous Monoethanolamine Solutions," *Chemical Engineering Research and Design* 100 (2015): 378–388.

30. É. S. Van-Dal and C. Bouallou, "Design and Simulation of a Methanol Production Plant From CO2 Hydrogenation," *Journal of Cleaner Production* 57 (2013): 38–45.

31. C. Roman and M. García-Morales, "Achieving a Better Understanding of Binary Azeotropic Mixtures Distillation Through Aspen Plus Process Simulations," *Computer Applications in Engineering Education* 27 (2019): 1453–1464, https://onlinelibrary.wiley.com/doi/pdf/10.1002/cae.22161.

32. A. Adil, A. M. Shivapuji, and L. Rao, "Thermodynamic Analysis for Methanol Synthesis Using Biomass-derived Syngas," *Biomass Conversion and Biorefinery* 12 (2022): 1819–1834.

33. J. Kurzke and I. Halliwell, *Propulsion and Power* (Springer International Publishing, 2018).

34. D. Laila, P. Shakouri, A. Ordys, and M. Askari, "Longitudinal Vehicle Dynamics Using Simulink/Matlab," in *UKACC International Conference on CONTROL 2010* (Institution of Engineering and Technology, 2010), 955–960.

35. P. Belotti, C. Kirches, S. Leyffer, J. Linderoth, J. Luedtke, and A. Mahajan, "Mixed-Integer Nonlinear Optimization," *Acta Numerica* 22 (2013): 1–131.

36. S. Mitra, I. E. Grossmann, J. M. Pinto, and N. Arora, "Optimal Production Planning Under Time-Sensitive Electricity Prices for Continuous Power-Intensive Processes," *Computers & Chemical Engineering* 38 (2012): 171–184.

37. W. F. Holmgren, C. W. Hansen, and M. A. Mikofski, "pvlib python: A Python Package for Modeling Solar Energy Systems," *Journal of Open Source Software* 3 (2018): 884.

38. Joint Research Centre - European Commission, "Photovoltaic Geographical Information System (PVGIS)," (2024).

39. Electricity Maps, "Carbon Intensity and Emission Factors," (2024), https://www.electricitymaps.com/methodology?utm_source=app.electricitymaps.com&;utm_medium=referral#carbon-intensity-and-emission-factors.

40. Gurobi Optimization LLC, "Gurobi Optimizer Reference Manual," (2025), https://www.gurobi.com/.

41. Fraunhofer-Institut für Solare Energiesysteme ISE, "Energy-Charts," (2025), https://www.energy-charts.info/index.html?l=de&c=DE.